The evolving radio jet from the neutron star X-ray binary 4U 1820-30

T. D. Russell, ^{1,2*} N. Degenaar, ² J. van den Eijnden, ³ M. Del Santo, ¹ A. Segreto, ¹ D. Altamirano, ⁴ A. Beri, ⁴ M. Díaz Trigo, ⁵ J. C. A. Miller-Jones ⁶

¹INAF, Istituto di Astrofisica Spaziale e Fisica Cosmica, Via U. La Malfa 153, I-90146 Palermo, Italy

Accepted 23-July-2021. Received 23-July-2021; in original form 23-July-2021

ABSTRACT

The persistently bright ultra-compact neutron star low-mass X-ray binary 4U 1820–30 displays a ~170 d accretion cycle, evolving between phases of high and low X-ray modes, where the 3 – 10 keV X-ray flux changes by a factor of up to \approx 8. The source is generally in a soft X-ray spectral state, but may transition to a harder state in the low X-ray mode. Here, we present new and archival radio observations of 4U 1820–30 during its high and low X-ray modes. For radio observations taken within a low mode, we observed a flat radio spectrum consistent with 4U 1820–30 launching a compact radio jet. However, during the high X-ray modes the compact jet was quenched and the radio spectrum was steep, consistent with optically-thin synchrotron emission. The jet emission appeared to transition at an X-ray luminosity of $L_{\rm X(3-10keV)} \sim 3.5 \times 10^{37} (D/7.6 \, {\rm kpc})^2 \, {\rm erg \, s^{-1}}$. We also find that the low-state radio spectrum appeared consistent regardless of X-ray hardness, implying a connection between jet quenching and mass accretion rate in 4U 1820–30, possibly related to the properties of the inner accretion disk or boundary layer.

Key words: accretion — stars: neutron — radio continuum: transients — X-rays: binaries — sources, individual: 4U 1820–30

1 INTRODUCTION

There is an observed phenomenological relationship between jet production and the accretion process in all accreting compact objects, however, at present the exact nature of the coupling remains to be determined. Neutron star (NS) and black hole (BH) low mass X-ray binary (LMXB) systems act as useful observational laboratories to study this coupling as they allow for the properties of the in-flowing accretion flow and out-flowing jets to be observed on human timescales. Changes in the accretion flow are typically observed in the X-rays, while corresponding changes in the jet emission are generally seen in the radio band. In particular, NS LMXBs offer an important observational tool allowing for the role that stellar surface, spin, and magnetic field play on jet production to be tested. However, due to the relative radio faintness of NS LMXBs (e.g., Gallo et al. 2018), our understanding of jet launching in NS LMXBs is generally less evolved than their BH counterparts (e.g., Migliari & Fender 2006).

Jets from accreting NS LMXBs show a diverse range of behaviour (e.g., Migliari & Fender 2006; Migliari 2011; Tudor et al. 2017; Gusinskaia et al. 2017; Gallo et al. 2018; Russell et al. 2018; Gusinskaia et al. 2020), and there has been some debate as to whether NS LMXB jets show a similar pattern of behaviour to BH systems (see, e.g., Migliari & Fender 2006; Marino et al. 2020). NS and

BH LMXBs can launch two types of jets depending on the state of the source: a steady compact jet or a bright transient jet (e.g., Migliari & Fender 2006), depending on the mass accretion rate (\dot{m}) and structure of the accretion flow. At lower \dot{m} during the harder Xray spectral states the compact jet is characterised by optically-thick synchrotron emission exhibiting a flat to inverted radio spectrum $(\alpha \sim 0)$, where the radio flux density, S_{ν} , is proportional to the observing frequency, ν , such that $S_{\nu} \propto \nu^{\alpha}$; Blandford & Königl 1979). At higher \dot{m} , when the source is softer, the compact jet emission can be quenched (Migliari et al. 2003; Tudose et al. 2009; Miller-Jones et al. 2010; Gusinskaia et al. 2017) and a transient jet is launched, although jet quenching is sometimes not observed (Rutledge et al. 1998; Kuulkers et al. 2003; Migliari et al. 2004; Migliari 2011). Recent results from BH LMXBs suggest that jet quenching at radio frequencies results as the jet spectral break, which is the break from optically-thick to optically-thin synchrotron emission for the highest energy synchrotron spectra, evolves below the radio band (e.g., Russell et al. 2020), implying that the jet acceleration region shifted away from the compact object (e.g., Markoff et al. 2001, 2005). A similar evolution of the jet spectral break is thought to occur in NS systems (Díaz Trigo et al. 2018). Around this time the short-lived, rapidly-flaring transient jet can be launched, exhibiting a steep radio spectrum ($\alpha \sim -0.7$) originating from ejected discrete (opticallythin) synchrotron emitting plasma (e.g., Fender 2006). Later, as the accretion rate reduces the source transitions back to the hard state and the compact jet re-establishes.

²Anton Pannekoek Institute for Astronomy, University of Amsterdam, Science Park 904, NL-1098 XH Amsterdam, The Netherlands

³Astrophysics, Department of Physics, University of Oxford, Denys Wilkinson Building, Keble Road, Oxford OX1 3RH, UK

⁴School of Physics and Astronomy, University of Southampton, Highfield SO17 IBJ, England

⁵ESO, Karl-Schwarzschild-Strasse 2, 85748 Garching bei München, Germany

⁶International Centre for Radio Astronomy Research - Curtin University, GPO Box U1987, Perth, WA 6845, Australia

^{*} E-mail:thomas.russell@inaf.it

4U 1820-30 is an ultra-compact NS LMXB located in the globular cluster NGC 6624, at ≈ 7.6 kpc (Kuulkers et al. 2003). This persistently X-ray bright object displays a ~170 d accretion cycle (e.g., Priedhorsky & Terrell 1984; Chou & Grindlay 2001), where the Xray luminosity evolves between $L_{low} \sim 8 \times 10^{36} (D/7.6 \, kpc)^2 \, erg \, s^{-1}$ and $L_{high} \sim 6 \times 10^{37} (D/7.6 \,\mathrm{kpc})^2 \,\mathrm{erg \, s^{-1}} \,\,(3-10 \,\mathrm{keV})$ (e.g., Priedhorsky & Terrell 1984; Šimon 2003; Wen et al. 2006), which we refer to as low and high X-ray modes, respectively. Generally in a soft X-ray state, 4U 1820-30 can sometimes transition to a hard state at its lowest mass accretion rates (during low modes, e.g., Tarana et al. 2007; Titarchuk et al. 2013).

Here, we present broadband radio observations of 4U 1820-30 taken during its high and low X-ray modes. Observations and analysis are given in Section 2. Section 3 reports the results from the radio observations and connecting the observed changes to the accretion flow. Conclusions are in Section 4.

2 OBSERVATIONS

2.1 Radio

All radio results are given in Table A1.

2.1.1 VLA

In total, we present eight radio observations of 4U 1820-30 from the Karl G. Jansky Very Large Array (VLA). The VLA observed 4U 1820-30 on 2018-12-09 (MJD 58461; project code 18A-194) and 2020-07-07 (MJD 59037; project code 20A-255), with data taken at L-band (1-2 GHz), C-band (4.5-5.5 and 7-8 GHz), and K-band (18-19 and 25-26 GHz), where all bands were observed within a 2-hour window but not simultaneously. For these radio observations 3C286 was used for bandpass and flux calibration, and J1820–2528 was used for phase calibration. The VLA also observed NGC 6624 five times between 2018 May 22 - 28 (MJDs 58260, 58261, 58262, 58265, and 58266) under project code 18A-081 (Shishkovsky et al. 2020). Those data were recorded at X-band (8 - 12 GHz), with durations of 1 or 2 hours. Flux and bandpass calibration were done using either 3C286 or 3C48 and phase calibration used J1820-2528. Due to flaring of 3C48 at the time of these VLA observations a 10% uncertainty was added in quadrature to the measured errors for those epochs.

Using the Common Astronomy Software Application (casa version 5.1.2; McMullin et al. 2007), data were edited for radio frequency interference (RFI) and systematics, before being calibrated following standard procedures. L-band and C-band observations were imaged with a Briggs robust parameter of 0 to balance sensitivity and resolution. K- and X-band data were imaged with natural weighting to maximise sensitivity. To characterise the radio spectral behaviour the L- and C-band observations were separated into 4×256 and 4×512 MHz sub-bands, respectively. The X-band observations were separated into 4×1 GHz sub-bands. The radio flux density of the target was determined by fitting for a point source in the image plane using a Gaussian with a full width half maximum set to the synthesised beam of the observation.

2.1.2 ATCA

The Australia Telescope Compact Array (ATCA) observed NGC 6624 on 2006-07-05 (MJD 53921), 2006-07-23 (MJD 53939), and 2006-08-08 (MJD 53955) under project code C1559. These observations were recorded simultaneously at 4.80 and 8.64 GHz, with

104 MHz of bandwidth at each central frequency. ATCA also observed the target field on 2015-04-24 (MJD 57136) and 2015-04-25 (MJD 57137) under project code C2877 (see Tremou et al. 2018, Tudor et al. in prep.). These two later observations were carried out at central frequencies of 5.5 and 9 GHz, and recorded using the Compact Array Broad-band Backend (CABB; Wilson et al. 2011) providing an increased bandwidth of 2 GHz at each central frequency. All ATCA observations used PKS 1934-638 for primary calibration and 1822-36 for phase calibration. Data were edited, calibrated, and imaged (using a natural weighting) as described above.

2.2 X-ray

2.2.1 MAXI, Swift-BAT, and RXTE-ASM

Daily count rates in the 2-20 keV band were obtained from the Monitor of All-sky X-ray Image (MAXI) X-ray telescope (Matsuoka et al. 2009) website¹. To estimate the X-ray flux at the time of the radio observations, we downloaded the X-ray spectral and rmf files from the MAXI website. The data were then analysed using xspec (version 12.8; Arnaud 1996) from the heasoft software package (version 6.21). Wilms et al. (2000) and Verner et al. (1996) were used to account for line-of-sight abundances and photoionisation cross sections. The 2 – 20 keV X-ray spectra were modelled with an absorbed power-law (tbabs \times powerlaw) within xspec. The $N_{\rm H}$ was fixed to 3×10^{21} cm⁻² (Bloser et al. 2000). The photon index was left free, resulting in best fits of ≈ 2 for all epochs (in agreement with results presented by Titarchuk et al. 2013). While more complex models are required to understand the accretion geometry of NS LMXBs, the low-sensitivity of the MAXI data and small changes in the X-ray spectrum over this energy range meant that the data are reasonably well fit by a simple absorbed power-law ($\chi^2 = 734$ with 685 degrees of freedom), such that they provided reasonable estimates on the 2 – 20 keV flux. More complex models provided similar fluxes.

Swift Burst Alert Telescope (Swift-BAT) Hard X-ray Transient Monitor (Krimm et al. 2013) daily count rates (15-50 keV) were obtained from the Swift-BAT website².

X-ray count rates from 2006 could not be obtained from MAXI as it was not yet employed. For these times, the Rossi X-ray Timing Explorer All-Sky Monitor (RXTE-ASM) 2–12 keV light curve was extracted from the ASM Light Curves webpage³.

http://maxi.riken.jp/top/index.html

https://swift.gsfc.nasa.gov/results/transients/

³ http://xte.mit.edu/ASM_lc.html

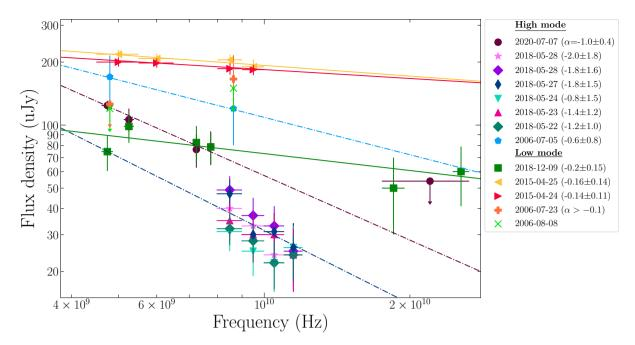


Figure 1. Radio emission from 4U 1820–30 during its high and low X-ray modes. All data are provided in Table A1. Fits to each epoch are shown, where dash-dotted lines were used for radio observations taken during high X-ray modes and solid lines were used for low X-ray modes. Radio spectral indices (α) for each epoch are provided in the legend. Due to the radio results showing little difference for the 2018 high mode data, for clarity, we only show the fit to these observations stacked together (which gives $\alpha = -1.32 \pm 0.54$). Non-detections are shown as three-sigma upper limits (determined as three times the image noise). For all observations, when the source was in a high X-ray mode the radio spectrum appeared steep ($\alpha \approx -1$), while during low X-ray modes the radio spectrum was flat ($\alpha \approx -0.15$), indicating a dramatic change in the jet between the X-ray modes.

3 RESULTS AND DISCUSSION

4U 1820–30 cycles between its high and low X-ray modes every ~170 days (e.g., Priedhorsky & Terrell 1984; Šimon 2003). The changes in the X-ray brightness are a consequence of an evolving mass accretion rate and accretion flow structure (Wijnands et al. 1999; Cornelisse et al. 2003; Zdziarski et al. 2007). This source is also a known radio emitter (e.g., Fruchter & Goss 2000; Migliari et al. 2004; Díaz Trigo et al. 2017). In this work, we report on radio observations of 4U 1820–30 taken during both its high and low X-ray modes showing a dramatic change in the observed jet emission.

3.1 X-ray modes and origin of the radio emission

To determine the X-ray mode of 4U 1820–30 at the time of the radio observations, we inspected *MAXI*, *Swift*-BAT and *RXTE*-ASM light curves, which clearly show the X-ray modulations (for example, see Figure A1). In almost all cases, *MAXI* data were used to determine the X-ray mode, where the mid-line between the maxima and minima of the periodic light curve occurs at a 2–20 keV *MAXI* count rate of ≈ 1 photons cm⁻² s⁻¹. For the three 2006 ATCA observations, the X-ray mode was estimated from count rates reported by Titarchuk et al. (2013).

Due to contamination from the nearby pulsar PSR 4U1820–30A ($\approx 0.22''$ away; Perera et al. 2017), we first explored the broadband 1–25 GHz radio emission from the source position with multifrequency VLA observations. Like Migliari et al. (2004), we find that the emission below 4 GHz is dominated by the nearby steep spectrum ($\alpha \sim -2$) radio pulsar, while higher radio frequencies show the flatter spectrum radio emission from 4U 1820–30 (Figure A2). Hereafter, we only discuss higher frequency (≈ 4 GHz) radio emission associated with 4U 1820–30.

3.2 An evolving radio jet between the high and low modes

Our broadband 4–26 GHz VLA observations of 4U 1820–30 taken in 2018 during a low X-ray mode show a relatively flat radio spectrum ($\alpha = -0.25 \pm 0.18$; Figure 1), consistent with optically-thick synchrotron emission from a self-absorbed compact jet. During the 2020 high X-ray mode the radio spectrum was steeper ($\alpha = -1.0 \pm 0.4$) and we did not detect radio emission at 22 GHz. This steep radio spectrum is consistent with optically-thin synchrotron emission indicating that the compact jet had switched off at these higher X-ray luminosities. The observed radio emission either originated from a quenched compact jet (where we are now seeing the optically-thin synchrotron emission), or from discrete jet ejecta in a transient radio jet (e.g., Fomalont et al. 2001; Fender et al. 2004; Migliari & Fender 2006). To determine if the jet changes are consistent for all high and low X-ray modes, we analysed archival VLA and ATCA radio observations (Figure 1).

3.2.1 Low X-ray modes

In addition to our 2018 VLA observation, there were four additional ATCA radio observations taken during low X-ray modes (two in 2006 and two in 2015). 4U 1820–30 was detected in both 2015 observations and one 2006 observation, exhibiting a relatively flat radio spectrum with radio spectral indices of $\alpha \sim -0.15$, consistent with a compact radio jet.

The 2015 ATCA observations of 4U 1820–30 were taken during a relatively hard X-ray spectral state, i.e., toward the typical island state (IS) of atoll sources (see Figure 2). These are the first reported radio detections from this source outside of the full soft state (as described by Titarchuk et al. 2013). Interestingly, while the jet emission may have been marginally brighter (by a factor of ~1.5

-2) at this time (see also Tremou et al. 2018), the radio spectrum ($\alpha \approx -0.15$) was consistent with other low X-ray mode radio observations. Further simultaneous radio and X-ray (spectral and timing) data are needed to accurately identify the X-ray state and to compare the radio emission.

For the two low-mode ATCA observations taken in 2006, the observations occurred prior to the ATCA bandwidth upgrade (Wilson et al. 2011) meaning that the sensitivity was poor and 4U 1820–30 was only detected in one frequency band (detected at 8.64 GHz but not at 4.8 GHz) on 2006-07-23, and not at all on 2006-08-08 (Figure 1). Using the 4.8 GHz upper-limit and 8.64 GHz detection implied a flat spectral index on 2006-07-23, where $\alpha > -0.1$.

3.2.2 High X-ray modes

For the high X-ray modes, we analysed an additional six VLA observations and two ATCA observations. In all cases where good constraints could be placed on the radio spectrum, the spectrum was steep such that $\alpha \sim -1$.

The six VLA observations were taken over 6 days in 2018, following an X-ray maximum as the X-ray brightness decreased. For all of these six VLA observations faint radio emission was detected from 4U 1820–30 (Figure 1). Unfortunately, the faintness of these detections meant that we were not able to identify any progressive changes to the radio emission (should they exist) between each epoch as the source evolved towards a low X-ray mode. While the measured radio spectrum of each individual epoch could have been consistent with ~flat, stacking these six observations together provided much tighter constraints on the spectral index, where $\alpha = -1.25 \pm 0.45$, inconsistent (at $\approx 2.9 \, \sigma$) with a flat radio spectrum.

ATCA also observed 4U 1820–30 during a high X-ray mode in 2006. Unfortunately, due to the low sensitivity of those radio observations we were unable to rule out a flat radio spectrum ($\alpha = -0.6 \pm 0.8$).

In addition, Díaz Trigo et al. (2017) reported on ATCA (5.5/9 GHz) and ALMA (302 GHz) observations from 2014, where the ALMA observations were taken 10 days prior to the ATCA observations. Those observations produced puzzling results, where 4U 1820-30 was detected at 5.5 and 302 GHz, but not at 9 GHz (despite the 5.5 and 302 GHz results indicating that the source should have been detected at 9 GHz). The 9 GHz non-detection was attributed to either atmospheric or systematic effects, or even an additional previously unknown bright millimetre (mm) source close to the position of 4U 1820-30 (to account for the bright 302 GHz emission). However, analysing the MAXI X-ray light curves at the time of the ATCA and ALMA observations revealed that, despite occurring only 10 days apart, the two jet observations occurred within different X-ray modes, where the ALMA observations were taken in a low mode and the ATCA taken in a high mode (corresponding to points 11 and 7, respectively, in Figure 2). Therefore, our results imply that the 9 GHz non-detection was a result of a steep radio spectrum at the time of the ATCA observations (using the $236 \,\mu\text{Jy}$ beam⁻¹5.5 GHz radio detection and assuming an $\alpha = -0.7$ radio spectrum, 4U 1820–30 should have been $\sim 167 \,\mu \rm Jy \, beam^{-1}$ at 9 GHz, below the 200 μJy beam⁻¹ upper-limit reported). The standalone ALMA data from Díaz Trigo et al. (2017) suggested a flat/inverted mm spectrum ($\alpha = 1.7 \pm 1.5$) with no strong intraobservational fading or brightening, implying emission from a compact jet. Comparing typical radio flux densities of 4U 1820-30 with the bright (400 μ Jy) ALMA detection suggests a radio to mm spectral index of ≥ 0.15 (as noted by Tremou et al. 2018).

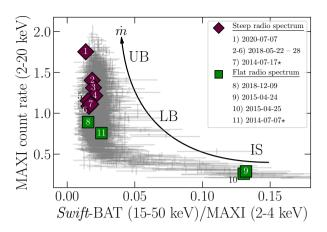


Figure 2. Hardness intensity diagram of 4U 1820–30 (grey markers), indicating the timing of radio observations. Magenta diamonds show radio observations with a steep radio spectrum, while the green squares represent a flat radio spectrum. The approximate location of the island (IS), lower banana (LB), and upper banana (UB) spectral branches are displayed (as depicted by Titarchuk et al. 2013), as well as the evolution of the mass accretion rate \dot{m} . The numbers correspond to each observational epoch (see legend). We include the ATCA (high mode) and ALMA (low mode) observations from Díaz Trigo et al. (2017), marked with a \star . The 2006 ATCA detections are not shown due to MAXI not being available, but support the conclusions here.

3.3 Quenching of the compact jet emission

Radio observations of 4U 1820-30 have shown a dramatic change in the jet emission between the source's high and low X-ray modes. These radio observations indicate that 4U 1820-30 launches a steady compact jet during its low X-ray modes but not during its high X-ray modes (Figure 1), indicating that the jet is quenched at those times. We also constrain the timescale of the jet quenching to be less than 10 days. For NS LMXBs, recent results have shown compact jet quenching occurring in less than 2 days (Díaz Trigo et al. 2018), with even shorter constraints for BH systems (Russell et al. 2020). No bright radio flaring was observed, where the observed 5 GHz radio flux densities only varied by a factor of \sim 2 for all observations. Therefore, while we currently favour a scenario where the high-mode steep-spectrum radio emission arises from the quenched compact jet (following the jet break evolving below the radio band as the jet's first acceleration zone moves away from the compact object; e.g., Russell et al. 2014), further high cadence radio observations (or sensitive high-resolution very long baseline interferometric radio observations) around the transition are required to identify whether this, or a transient jet are responsible for the observed radio emission. At present, the shortest timescale we can place on the launching, flaring, and fading of any transient jet ejecta is ≤ 10 days (see Section 3.2.2).

3.3.1 Connection to the accretion flow

In BH transients, compact jet quenching is typically associated with a transition from the hard to the soft X-ray spectral state. In NS LMXBs, in particular in atoll-type sources, the jet quenching scenario is not so clear, with the jet quenching observed in some sources, but not others (e.g., Migliari 2011; Gusinskaia et al. 2017, for further discussion). In 4U 1820–30, we have observed compact jet quenching that appears to be strongly connected with the accretion rate, where the jet emission transformed at an X-ray flux of

 $\sim 5.1 \times 10^{-9} \text{erg s}^{-1} \text{ cm}^{-2}$ (3–10 keV), corresponding to a transition luminosity of $\sim 3.5 \times 10^{37} (D/7.6 \text{ kpc})^2 \text{ erg s}^{-1} (3-10 \text{ keV})$.

Connecting the observed source evolution with the typical atoll-type spectral branches: at its lowest mass accretion rate 4U 1820–30 the X-ray spectrum is hardest (within the IS; Figure 2), then as the average mass accretion rate increases the source initially softens before rising at a constant hardness through the lower banana (LB) to the upper banana (UB) branch, with the transition of the jet occurring somewhere around the LB state (Figure 2). In atoll-type sources as the mass accretion rate rises (from the LB to UB branch), the electron temperature of the Comptonising medium (the boundary layer) remains almost constant while the optical depth increases. A change in the boundary layer, along with a simultaneous decrease of the inner disk radius (e.g., Gierliński & Done 2002) could be responsible for the jet changes.

In comparison, in Z-type NS LMXBs, which only show soft X-ray states (but do show some changes in the X-ray hardness), the NS black-body temperature increases by a factor of \sim 2 when \dot{m} rises within the normal branch, giving an increase of the radiation pressure. Moreover, transient radio jets are launched during this progression (Migliari & Fender 2006). In a unified model for NS LMXBs, Church et al. (2014) proposed that in both atoll and Z-type sources an increase of the radiation pressure may be responsible for disrupting the inner disk and launching transient jets, implying a connection between the jets and the inner accretion disk.

A possible coupling between the jet emission and the boundary layer is an interesting prospect. Such a connection was discussed in a study of the dwarf nova SS Cyg, where the observed radio emission brightened around the time that material first reached the boundary layer and radio flaring was observed when the optical depth of the boundary layer increased such that it became optically-thick to itself (Russell et al. 2016). That study speculated that the boundary layer may provide a vertically-extended region required for jet launching, analogous to BH and NS LMXBs, where the WD and NS systems have a boundary layer while BH LMXBs contain a geometrically-thick accretion flow (i.e., corona; e.g., Zdziarski & Gierliński 2004).

4 CONCLUSIONS

4U 1820-30 periodically cycles between high and low X-ray accretion modes. Using new and archival radio observations of this system during each of these modes, we report on dramatic changes to the jet emission. In all observations where good constraints could be placed on the radio spectrum, 4U 1820-30 launched a flat-spectrum compact jet during its low X-ray modes, which was quenched during the high X-ray modes. In the latter case, the radio spectrum was consistent with optically-thin synchrotron emission from either a quenched compact jet where the jet break had evolved below the radio band jet, or possibly a transient jet. The changes in the jet appear to be strongly linked to the X-ray luminosity, and hence the mass accretion rate, suggesting a connection to the composition of the inner accretion flow or boundary layer and not the X-ray spectral state. The observations reported here suggest that the radio emission transforms rapidly at an X-ray luminosity of $L_{\rm X(3-10\,keV)} \sim 3.5 \times 10^{37} (D/7.6\,{\rm kpc})^2 {\rm erg \, s^{-1}}$. High cadence radio and X-ray observations around and after the transition are required to determine precisely when the jet transition occurs, discriminate between the quenched compact jet and transient jet scenario, and identify the specific changes in the accretion flow that may be driving the jet evolution. In particular, X-ray monitoring that includes spectral and X-ray timing information is necessary.

ACKNOWLEDGEMENTS

We thank the referee for their helpful comments. TDR, MDS and AS acknowledge financial contribution from ASI-INAF n.2017-14-H.0, an INAF main stream grant. ND is supported by a Vidi grant from the Dutch organization for scientific research (NWO). JvdE is supported by a Lee Hysan Junior Research Fellowship from St Hilda's College, Oxford. The NRAO is a facility of the NSF operated under cooperative agreement by Associated Universities, Inc. ATCA is part of the ATNF which is funded by the Australian Government for operation as a National Facility managed by CSIRO. We acknowledge the Gomeroi people as the traditional owners of the ATCA observatory site. This research made use of NASA's Astrophysics Data System, software, and HEASARC web tools, and MAXI, Swift-BAT and RXTE-ASM data.

DATA AVAILABILITY

All radio results are provided in Table A1. VLA, ATCA, and ALMA data can be accessed from their online archives. *MAXI*, *Swift*-BAT, and *RXTE*-ASM light curves are publicly available.

REFERENCES

Arnaud K. A., 1996, in Jacoby G. H., Barnes J., eds, Astronomical Society of the Pacific Conference Series Vol. 101, Astronomical Data Analysis Software and Systems V. p. 17

Blandford R. D., Königl A., 1979, ApJ, 232, 34

Bloser P. F., Grindlay J. E., Kaaret P., Zhang W., Smale A. P., Barret D., 2000, ApJ, 542, 1000

Chou Y., Grindlay J. E., 2001, ApJ, 563, 934

Church M. J., Gibiec A., Bałucińska-Church M., 2014, MNRAS, 438, 2784 Cornelisse R., et al., 2003, A&A, 405, 1033

Díaz Trigo M., Migliari S., Miller-Jones J. C. A., Rahoui F., Russell D. M., Tudor V., 2017, A&A, 600, A8

Díaz Trigo M., et al., 2018, A&A, 616, A23

Fender R., 2006, Jets from X-ray binaries. Cambridge University Press, Cambridge, pp 381–419

Fender R., Wu K., Johnston H., Tzioumis T., Jonker P., Spencer R., van der Klis M., 2004, Nature, 427, 222

Fomalont E. B., Geldzahler B. J., Bradshaw C. F., 2001, ApJ, 553, L27

Fruchter A. S., Goss W. M., 2000, ApJ, 536, 865

Gallo E., Degenaar N., van den Eijnden J., 2018, MNRAS, 478, L132

Gierliński M., Done C., 2002, MNRAS, 337, 1373

Gusinskaia N. V., et al., 2017, MNRAS, 470, 1871

Gusinskaia N. V., et al., 2020, MNRAS, 492, 2858

Krimm H. A., et al., 2013, ApJS, 209, 14

Kuulkers E., den Hartog P. R., in't Zand J. J. M., Verbunt F. W. M., Harris W. E., Cocchi M., 2003, A&A, 399, 663

Marino A., et al., 2020, MNRAS, 498, 3351

Markoff S., Falcke H., Fender R., 2001, A&A, 372, L25

Markoff S., Nowak M. A., Wilms J., 2005, ApJ, 635, 1203

Matsuoka M., et al., 2009, PASJ, 61, 999

McMullin J. P., Waters B., Schiebel D., Young W., Golap K., 2007, in Shaw R. A., Hill F., Bell D. J., eds, Astronomical Society of the Pacific Conference Series Vol. 376, Astronomical Data Analysis Software and Systems XVI. p. 127

Migliari S., 2011, in Romero G. E., Sunyaev R. A., Belloni T., eds, Jets at All Scales. 275. pp 233–241, doi:10.1017/S174392131001608X

Migliari S., Fender R. P., 2006, MNRAS, 366, 79

Migliari S., Fender R. P., Rupen M., Jonker P. G., Klein-Wolt M., Hjellming R. M., van der Klis M., 2003, MNRAS, 342, L67

Migliari S., Fender R. P., Rupen M., Wachter S., Jonker P. G., Homan J., van der Klis M., 2004, MNRAS, 351, 186

```
Miller-Jones J. C. A., et al., 2010, ApJ, 716, L109
Perera B. B. P., et al., 2017, MNRAS, 468, 2114
Priedhorsky W., Terrell J., 1984, ApJ, 284, L17
Russell T. D., Soria R., Miller-Jones J. C. A., Curran P. A., Markoff S., Rus-
    sell D. M., Sivakoff G. R., 2014, MNRAS, 439, 1390
Russell T. D., et al., 2016, MNRAS, 460, 3720
Russell T. D., Degenaar N., Wijnands R., van den Eijnden J., Gusinskaia
    N. V., Hessels J. W. T., Miller-Jones J. C. A., 2018, ApJ, 869, L16
Russell T. D., et al., 2020, MNRAS, 498, 5772
Rutledge R., Moore C., Fox D., Lewin W., van Paradijs J., 1998, The As-
    tronomer's Telegram, 8, 1
Shishkovsky L., et al., 2020, ApJ, 903, 73
Tarana A., Bazzano A., Ubertini P., Zdziarski A. A., 2007, ApJ, 654, 494
Titarchuk L., Seifina E., Frontera F., 2013, ApJ, 767, 160
Tremou E., et al., 2018, ApJ, 862, 16
Tudor V., et al., 2017, MNRAS, 470, 324
Tudose V., Fender R. P., Linares M., Maitra D., van der Klis M., 2009, MN-
    RAS, 400, 2111
Verner D. A., Ferland G. J., Korista K. T., Yakovlev D. G., 1996, ApJ, 465,
Wen L., Levine A. M., Corbet R. H. D., Bradt H. V., 2006, ApJS, 163, 372
Wijnands R., Homan J., van der Klis M., 1999, ApJ, 526, L33
Wilms J., Allen A., McCray R., 2000, ApJ, 542, 914
Wilson W. E., et al., 2011, MNRAS, 416, 832
Zdziarski A. A., Gierliński M., 2004, Progress of Theoretical Physics Sup-
    plement, 155, 99
Zdziarski A. A., Gierliński M., Wen L., Kostrzewa Z., 2007, MNRAS, 377,
Šimon V., 2003, A&A, 405, 199
```

APPENDIX A: ONLINE INFORMATION: LIGHT CURVES, AND RADIO SEDS, AND RADIO DATA

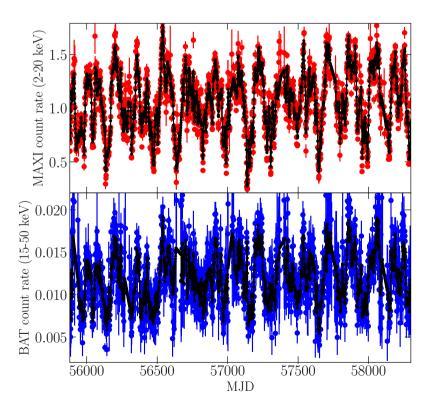


Figure A1. X-ray light curves of 4U 1820–30, showing an example of the X-ray periodicity. The top panel shows the *MAXI* daily 2–20 keV count rate, while the lower panel shows the *Swift*-BAT 15–50 keV rate. The coloured points show the reported rates, while the black points/line gives the 5-day moving average. The X-ray modulations of 4U 1820–30 are clearly visible.

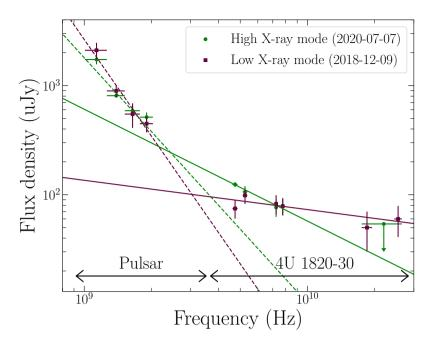


Figure A2. Radio emission from the source position of $4U\ 1820-30$ showing the contribution from nearby pulsar PSR $4U\ 1820-30$ to the emission ($\approx 0.2''$ away). These observations - taken during both the high (black circles) and low X-ray modes (red squares) show that $4U\ 1820-30$ dominates at frequencies above $4\ GHz$, while the radio pulsar dominated the emission at lower frequencies. Fits to the pulsar data are shown by the dashed lines, while the LMXB is shown with solid lines.

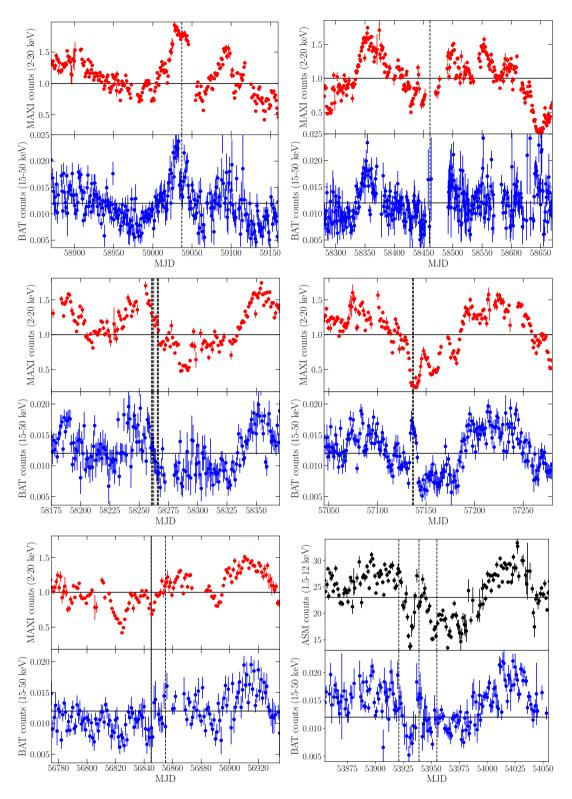


Figure A3. X-ray light curves of 4U 1820–30 around the timing of the radio observations discussed in this paper. The top panel of each figure shows the MAXI 2–20 keV light curves, while the lower panel is the 15–50 keV Swift-BAT light curve. Vertical dashed lines show the timing of the radio observations. Solid horizontal lines shows the approximate mid-line of the light curves. (Top left): VLA observation taken during the 2020 high X-ray mode. (Top right): 2018 low mode. (Middle left): Timing of the six close-in-time 2018 high mode observations, taken as 4U 1820–30 fades from an X-ray peak. (Middle right): Radio observations taken on two consecutive days during its 2015 low mode. These two radio observations were taken in a harder X-ray state. (Lower left): ALMA (solid vertical line) and ATCA (dashed vertical line) from 2014 taken during a low and high X-ray mode, respectively (from Díaz Trigo et al. 2017). (Lower right): RXTE-ASM and Swift-BAT light curves during the 2006 ATCA radio observations, with one high-mode (the first) and two low-mode observations (second and third).

Table A1. Radio observations of 4U 1820-30 during its high and low X-ray modes. Low frequency (< 4 GHz) results are attributed to the nearby pulsar (PSR 1820-30A) and higher radio frequencies are 4U 1820-30. Observations taken in the high X-ray mode are presented in the top panel, while the those taken in the low X-ray mode are in the lower panel. Errors are $1-\sigma$ and upper-limits are $3-\sigma$. Flux density errors include systematic uncertainties.

Date	MJD	Project code	Frequency (GHz)	Flux density (μJy)	α	3-10 keV X-ray flux $\times 10^{-9} \text{ erg/s}$	X-ray mode/sta
2020-07-07	59037.22 ± 0.03	20A-255	1.1355	1730 ± 165	-2.2 ± 0.3		Pulsar
			1.3915	810 ± 50			
			1.6475	590 ± 70			
			1.9035	515 ± 55			
			4.743	124 ± 14	-1.0 ± 0.4	8.05 ± 0.20	High/Soft
			5.255	106 ± 14			
			7.243	76 ± 14			
			7.755	78 ± 15			
			22.00	< 54			
2018-05-28	58266.457 ± 0.015	18A-081	8.488	40 ± 9	-2.0 ± 1.9	5.13 ± 0.15	High/Soft
			9.488	33 ± 8			
			10.488	24.0 ± 8.5			
			11.488	25.0 ± 8.5			
2018-05-28	58266.313 ± 0.015	18A-081	8.488	44 ± 8	-1.8 ± 1.6	5.13 ± 0.15	High/Soft
			9.488	38 ± 9			
			10.488	33 ± 9			
	50065 465 0 015	104 001	11.488	25 ± 8	10 15	60.07	TT: 1 /G .C.
2018-05-27	58265.467 ± 0.015	18A-081	8.488	38 ± 8	-1.8 ± 1.5	6.2 ± 0.7	High/Soft
			9.488	30 ± 8			
			10.488	31 ± 7			
	50060 45 0 0 4	104 001	11.488	26 ± 8	0.0 1.5	50.02	TT: 1 /G 6:
2018-05-24	58262.47 ± 0.04	18A-081	8.488	31 ± 6	-0.8 ± 1.5	5.9 ± 0.2	High/Soft
			9.488	25 ± 6			
			10.488	22 ± 6			
2018-05-23	59261 401 + 0.015	10 4 001	11.488	26 ± 7	14.12	6.07 + 0.14	II: -1- /C - 6-
	58261.491 ± 0.015	18A-081	8.488	35 ± 8	-1.4 ± 1.3	6.07 ± 0.14	High/Soft
			9.488	28 ± 6			
			10.488	22 ± 6			
2019 05 22	50260 47 + 0.04	10 4 001	11.488	24.0 ± 6.5	12 : 10	(05 + 0.16	II: -1-/C - 6-
2018-05-22	58260.47 ± 0.04	18A-081	8.488	32 ± 5	-1.2 ± 1.0	6.05 ± 0.16	High/Soft
			9.488	28.0 ± 5.5			
			10.488	22.0 ± 5.5			
2014 07 174	E (0 E E	C2010	11.488	24 ± 6	. 0.1	40 . 06	II: -1-/C - 6-
2014-07-17 ^a	56855	C3010	5.5 9.0	236 ± 27 < 200	< -0.1	4.9 ± 0.6	High/Soft
2006-07-05	53921.57 ± 0.24	C1559	4.8	170 ± 45	-0.6 ± 0.8	7.0 ± 0.7^{b}	High/Soft
2000-07-03	33921.37 ± 0.24	C1339	8.64	170 ± 43 130 ± 40	-0.0 ± 0.8	7.0 ± 0.7	Trigh/Soft
2018-12-09	58461.81 ± 0.03	18A-194	1.1355	2000 ± 450	-2.7 ± 0.7		Pulsar
			1.3915	890 ± 110			
			1.6475	550 ± 140			
			1.9035	450 ± 75			
			4.743	75 ± 14	-0.25 ± 0.18	3.76 ± 0.35	Low/Soft
			5.255	98 ± 17			
			7.243	83 ± 17			
			7.755	79 ± 15			
			18.5	50 ± 20			
			25.5	62 ± 19			
2015-04-24	57136.76 ± 0.20	C2877	5.0	200 ± 10	-0.14 ± 0.11	1.23 ± 0.15	Low/Harde
			6.0	198 ± 10			
			8.5	186 ± 12			
			9.5	184 ± 11			
2015-04-25	57137.78 ± 0.22	C2877	5.0	218 ± 11	-0.16 ± 0.14	1.20 ± 0.15	Low/Harde
			6.0	208 ± 11			
			8.5	205 ± 12			
201/2= :=:			9.5	190 ± 16	. –		_
2014-07-07 ^a	56845	ALMA	295	390 ± 25	1.7 ± 1.5	3.0 ± 0.6	Low/Soft
			297	404 ± 26			
			307	415 ± 28			
	F000*	A	309	440 ± 28		ما≕ى تىمىس	
2006 27 11	52020 FO + 0 24	C1559	4.8	< 126	> -0.1	5.26 ± 0.5^{b}	Low/Soft
2006-07-23	53939.50 ± 0.24						
		G1.550	8.64	166 ± 50		4.77 o 5h	T '0 0
2006-07-23 2006-08-08 S 000 , 1- ?? (20	53955.50 ± 0.23	C1559	8.64 4.8 8.64	166 ± 50 < 120 < 150	_	$4.7\pm0.5^{\rm b}$	Low/Soft